The Journal of Chemical Physics

RESEARCH ARTICLE | NOVEMBER 03 2026

Electrowetting: Contact angle saturation induced by non-local surface excess free energy

Ruize Yin ; Fei Wang ; Britta Nestler

Check for updates

J. Chem. Phys. 165, 174706 (2026)
https://doi.org/10.1063/5.0353545

View Online
Export Citation

Articles You May Be Interested In

Electrowetting on thick substrates: A modified Young–Lippmann equation
J. Chem. Phys. (July 2026)

Numerical investigation of electrowetting-based droplet splitting in closed digital microfluidic system: Dynamics, mode, and satellite droplet
Physics of Fluids (November 2018)

Nonwoven electrowetting textiles
Appl. Phys. Lett. (July 2007)

09 November 2026 06:57:17

AIP Publishing
The Journal of Chemical Physics
Special Topics Open for Submissions
Learn More

AIP Publishing

The Journal of Chemical Physics ARTICLE pubs.aip.org/aip/jcp

Electrowetting: Contact angle saturation induced by non-local surface excess free energy

Cite as: J. Chem. Phys. 165, 174706 (2026); doi: 10.1063/5.0353545
Submitted: 22 July 2026 • Accepted: 19 October 2026 •
Published Online: 3 November 2026

View Online Export Citation CrossMark

Ruize Yin,[1,2] Fei Wang,[1,2,a)] and Britta Nestler[1,2,3]

AFFILIATIONS

[1] Institute for Applied Materials, Microstructure Modelling and Simulation (IAM-MMS), Karlsruhe Institute of Technology (KIT), Strasse am Forum 7, 76131 Karlsruhe, Germany
[2] Institute of Nanotechnology (INT), Karlsruhe Institute of Technology (KIT), Hermann-von-Helmholtz-Platz 1, 76344 Eggenstein-Leopoldshafen, Germany
[3] Institute of Digital Materials Science, Karlsruhe University of Applied Sciences, Moltkestrasse 30, 76133 Karlsruhe, Germany

[a)] **Author to whom correspondence should be addressed:** fei.wang@kit.edu

ABSTRACT

Contact-angle saturation limits the high-voltage response of electrowetting-on-dielectric systems, but it is not captured by the classical Young–Lippmann relation. Here, we develop a composition-dependent interfacial energy-landscape model in which the liquid-covered and gas-covered parts of the substrate are described by adsorption-layer states with composition-dependent free energies and capacitive responses. The Young–Lippmann behavior is recovered at low voltage, while saturation emerges when the gas-covered adsorption layer becomes liquid-rich and the electrical contributions to the solid–liquid and solid–gas interfacial free energies decrease synchronously. The model provides analytical expressions for the onset voltage, saturation voltage, and saturated contact angle and separates the voltage scale from the terminal interfacial-energy contrast. Comparison with experimental data shows that the normalized electrowetting response is consistent with the proposed interfacial transition pathway. The resulting energy landscape can also contain metastable states, giving rise to path-dependent behavior during voltage withdrawal. Together, these results indicate that variations in the underlying interfacial parameters can regulate both the terminal wetting state and the overall electrowetting response.

© 2026 Author(s). All article content, except where otherwise noted, is licensed under a Creative Commons Attribution (CC BY) license (https://creativecommons.org/licenses/by/4.0/). https://doi.org/10.1063/5.0353545

09 November 2026 06:57:17

I. INTRODUCTION

Electrowetting enables electrical control of the apparent wettability of conducting or electrolytic liquids and is widely used in digital microfluidics, adaptive optics, displays, and other droplet-based devices.[1,2] In the ideal electrowetting-on-dielectric (EWOD) case, a conducting droplet and the underlying electrode form a capacitor separated by an insulating coating. For a prescribed voltage, the appropriate electrical contribution to the thermodynamic potential is $-cV^2/2$ per unit wetted area, where c is the areal capacitance of the electrically active stack. Combining this contribution with Young's relation gives the Young–Lippmann equation,

$$\cos\theta(V) = \cos\theta_0 + \frac{cV^2}{2\gamma_{LG}}, \tag{1}$$

which accurately describes the initial quadratic response of many EWOD systems.[1,3] This macroscopic relation should be interpreted in terms of an apparent contact angle: electrostatic stresses strongly deform the interface over distances comparable with the dielectric thickness, whereas the microscopic angle sufficiently close to the contact line can remain close to the zero-field Young angle.[4,5]

The Young–Lippmann relation cannot remain valid indefinitely because it predicts complete wetting and, upon further extrapolation, the nonphysical condition $\cos\theta > 1$. Experiments instead commonly show a reduced voltage sensitivity, followed by an apparent plateau, usually termed contact-angle saturation. Depending on the materials, ambient phase, voltage protocol, and observation time, the same high-field range may also display contact-angle hysteresis, residual charging, leakage current, contact-line corrugation, droplet ejection, or dielectric failure.[6,7] These phenomena should not be treated as synonymous. Contact-angle saturation denotes the limiting macroscopic wetting response, whereas hysteresis and irreversible charging characterize path dependence, and breakdown or ejection represent loss of the ideal equilibrium EWOD state. It

is, therefore, important to distinguish whether a given description addresses an equilibrium wetting limit, a kinetic charging process, or a material-instability threshold.

Several mechanisms can limit the high-voltage response. Verheijen and Prins introduced trapped interfacial charge as a screening field and reproduced a threshold beyond which the effective electrowetting voltage ceased to increase.[8] Subsequent electrohydrostatic calculations and leakage-current measurements connected saturation to the intense edge field near the contact line, local dielectric breakdown, and the associated accumulation of trapped charge.[9–11] In air, Vallet, Vallade, and Berge observed gas ionization and electrical discharge near the drop edge and showed that the resulting charge deposition can suppress the electrowetting driving force.[12] For droplets immersed in a weakly conducting surrounding liquid, ion transfer from the droplet to the ambient phase can reduce the Maxwell traction and add an osmotic contribution, producing a broad minimum or an apparent saturation of the contact angle.[13] These approaches identify physically well-motivated routes to saturation and are particularly valuable when current, polarity effects, residual charge, discharge, or material damage are measured. Their applicability, however, depends on the relevant charge-transfer pathway, dielectric strength, ambient phase, and time scale; none of these mechanisms should be assumed to operate identically in every EWOD configuration.[1,7]

A complementary class of theories retains an equilibrium or quasi-equilibrium description but modifies the high-voltage free energy. Thermodynamic-limit models associate saturation with a lower bound on the effective solid–liquid interfacial free energy.[14,15] Geometry-based formulations instead treat the electric energy as a global function of droplet shape and counter-electrode configuration; then, an electric-energy minimum can yield saturation and, under other conditions, reverse electrowetting.[16] More general variational relations emphasize that the apparent angle is controlled by the variation of electrical capacitance with contact-line displacement rather than by a spatially uniform capacitor alone.[17] These models are useful because they provide closed macroscopic relations without requiring a detailed account of irreversible material failure. Nevertheless, the high-voltage closure is generally introduced through a limiting interfacial energy, a prescribed geometry-dependent electric-energy function, or an effective capacitance law. The internal interfacial state that evolves between the Young–Lippmann regime and the terminal state is, therefore, often not represented as an independent thermodynamic variable.

More spatially resolved electrostatic and electrohydrodynamic descriptions account for interfacial charging and ionic redistribution,[18–20] including diffuse-layer and finite-size charging effects,[21,22] as well as nonuniform electric fields and interface deformation under electrowetting conditions.[23–25] Molecular simulations have further shown that strong local electric fields and ion transfer can produce a Young–Lippmann-like regime, followed by saturation at nanoscopic scales.[26] Such approaches provide detailed microscopic or spatially resolved mechanisms, whereas the present work adopts a reduced interfacial thermodynamic description in which these unresolved electrical effects are represented through effective state-dependent interfacial properties.

Local contact-line descriptions and global free-energy formulations should not be regarded as mutually exclusive approaches to wetting. A familiar example is Young's law, which can be obtained either from a local force balance at the three-phase contact line[27] or from minimization of the total interfacial free energy.[28,29] Similarly, electrowetting can be formulated in terms of the local electrical contribution in the vicinity of the contact line,[17] while an equivalent macroscopic description may be constructed through the variation of the total interfacial free energy.

Following this thermodynamic viewpoint, we coarse-grain the unresolved local effects in the vicinity of the three-phase contact line into effective surface free-energy contributions. The schematic interfacial region shown in Fig. 1(b) is conceptually inspired by the "core region" introduced by de Gennes, within which the microscopic interfacial structure may be considerably more complex than the apparent macroscopic geometry.[30] Our adsorption-layer description extends this idea by representing the thermodynamic influence of this unresolved region through averaged interfacial state variables and their corresponding excess free-energy contributions.

The preceding work leaves room for a reduced interfacial thermodynamic description of a distinct hypothesis: the applied voltage may modify not only the interfacial state beneath the macroscopic liquid footprint but also a finite droplet-affected transition region immediately outside the apparent contact line. Such a region may contain unresolved variations in composition, geometry, polarization, and charge storage that are not represented by a sharp macroscopic solid–liquid/solid–gas boundary. Existing adaptive-wetting and diffuse-interface descriptions demonstrate more generally that a solid-adjacent region can possess a composition-dependent excess free energy rather than acting as a structureless geometrical boundary.[31–33] What is still insufficiently clarified for this hypothesis is whether a small set of bounded interfacial state variables can connect the low-voltage Young–Lippmann response, the onset of deviation, and a terminal apparent angle while separating the parameters that set the voltage scale from those that set the final interfacial-energy contrast.

Here, we develop a composition-dependent interfacial energy-landscape model for this purpose. The liquid-covered and neighboring gas-covered but liquid-affected parts of the substrate are characterized by the coarse-grained wetting-state variables ϕ_L and ϕ_G, respectively. These variables are defined as the surface-area averages of the local solid-adjacent composition φ_s over the corresponding interfacial regions,

$$\phi_L = \frac{1}{A_{SL}} \int_{A_{SL}} \varphi_s(\mathbf{x})\, \mathrm{d}A, \tag{2}$$

$$\phi_G = \frac{1}{A_{SG} - A_{SL}} \int_{A_{SG}-A_{SL}} \varphi_s(\mathbf{x})\, \mathrm{d}A. \tag{3}$$

Here, φ_s denotes the local composition at the solid-adjacent interface, while ϕ_L and ϕ_G represent its coarse-grained averages over the liquid-covered and neighboring gas-covered regions, respectively.

Their chemical free energies are combined with a composition-dependent effective capacitance, and the electrical contribution under the fixed-voltage condition is written as $-\int_0^V \sigma(\phi, V')\, \mathrm{d}V'$. Minimization of the resulting free-energy landscape determines the adsorption-layer state and the associated apparent contact angle. The classical Young–Lippmann response is recovered when ϕ_L remains liquid-rich, ϕ_G remains gas-rich, and the liquid-side

09 November 2026 06:57:17

© Author(s) 2026

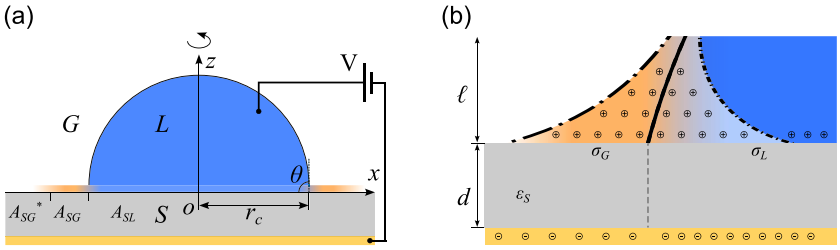


FIG. 1. Schematic of the electrowetting system with a composition-dependent adsorption layer. A sessile droplet (L) rests on a dielectric-coated solid substrate (S) in a surrounding gas phase (G). (a) Macroscopic droplet geometry. The apparent contact angle and contact radius are denoted by θ and r_c, respectively. The droplet-affected region A_{SG} consists of the liquid-covered area A_{SL} and the neighboring gas-covered region $A_{SG} - A_{SL}$ near the apparent three-phase contact line. The far-field gas-covered region A_{SG}^* is assumed to remain unaffected. (b) Enlarged view of the local interfacial structure under an applied voltage V. The dielectric coating has thickness d and permittivity ε_S. The color-gradient region enclosed by two dashed curves represents the interfacial transition region near the three-phase contact line, which is coarse-grained into an effective adsorption layer of thickness ℓ. The solid curve represents the ideal spherical-cap interface defined by the macroscopic apparent contact angle. The effective surface charge densities in the liquid-covered and neighboring gas-covered regions are denoted by σ_L and σ_G, respectively. The representation of the contact-line region in panel (b) is conceptually inspired by the "core region" discussed by de Gennes.[30]

effective capacitance is approximately constant. Deviation begins when the gas-side boundary loses local stability, and a terminal state is reached when the bounded variable ϕ_G attains its liquid-rich limit. Under the explicit constitutive assumption that the liquid-rich limits of the two regions have the same effective capacitance, their voltage-dependent electrical terms cancel from the interfacial-energy difference, producing a voltage-independent apparent contact angle. The model then provides analytical local thresholds for the onset and terminal boundaries and distinguishes the capacitance-controlled voltage scale from the terminal chemical free-energy contrast. Comparison with normalized experimental data is used to test the consistency of this transition pathway, rather than to exclude charge trapping, breakdown, ion injection, or other high-field mechanisms that may dominate in particular devices.

The introduction of an adsorption layer should not be interpreted as assuming the existence of a distinct, macroscopically resolvable layer of liquid or gas beneath either the droplet or the surrounding gas phase. Rather, it provides a coarse-grained description of the highly complex interfacial region in the vicinity of the three-phase contact line, where strong spatial variations in composition and molecular organization may occur. The liquid-rich limit $\phi_G = 1$, therefore, denotes the terminal state of the coarse-grained interfacial variable and should not be interpreted as a macroscopically continuous aqueous film of thickness ℓ.

The complexity of this near-contact-line region is evident at multiple scales in both conventional wetting and electrowetting systems.[34] Buehrle, Herminghaus, and Mugele showed that the electrostatic field in electrowetting produces a strongly nonuniform liquid–gas interface profile near the three-phase contact line, with the local contact angle approaching Young's angle in the immediate vicinity of the substrate while evolving toward the apparent Lippmann angle farther away.[4] The characteristic region over which this interfacial deformation occurs is of the order of the dielectric thickness, although the electrostatic disturbance exhibits an algebraically decaying spatial structure. Such results illustrate that the local state near the contact line can contain substantially more spatial information than is retained in a macroscopic contact-angle description.

At these small-scale investigations, molecular simulations[35] have revealed molecularly thin precursor films extending beyond the apparent contact line, whereas experimental studies[36,37] have also observed liquid films outside the macroscopic droplet footprint, in some cases with a thickness sufficiently large to be directly resolved. The precursor- and trailing-film observations cited above establish the plausibility of non-bulk interfacial material outside the apparent contact line, but they do not constitute direct evidence for the equilibrium electrically coupled state assumed in the present model. These observations nevertheless indicate that the local composition near the contact line is unlikely to conform strictly to the idealized picture of a purely liquid-covered solid beneath the droplet and a purely gas-covered solid immediately outside it.

The adsorption-layer theory introduced here is not intended to explicitly resolve these microscopic or macroscopic precursor or trailing films, nor their detailed geometries. Instead, it provides a thermodynamically consistent mean-field description in which the complex local interfacial phenomena are captured by an effective energetic contribution. This enables their impact on the macroscopic wetting behavior of the droplet to be incorporated into the free-energy formulation.

II. METHOD

A. Derivation of Young's law and the Young–Lippmann equation

We first recall the classical variational derivation of Young's law for a liquid droplet of fixed volume Ω resting on a flat, smooth, and horizontal solid substrate, surrounded by a gas phase. The surface free energy of the system is written as

$$E = \gamma_{LG}A_{LG} + \gamma_{SL}A_{SL} + \gamma_{SG}(A_{SG} - A_{SL}) + \gamma_{SG}^*A_{SG}^*. \tag{4}$$

Here, γ_{LG} is the liquid–gas interfacial free-energy density, while γ_{SL} and γ_{SG} denote the solid–liquid and solid–gas interfacial free-energy densities in the droplet-affected region, respectively. These two interfacial free energies may depend on the local wetting state and, in the electrowetting problem considered in the following, on

09 November 2026 06:57:17

© Author(s) 2026

the externally applied voltage. By contrast, γ_{SG}^{*} denotes the far-field solid–gas interfacial free-energy density outside the droplet-affected region. This far-field contribution is assumed to be independent of the droplet shape, the wetting state, and the electric field and is, therefore, treated as a constant reference contribution.

In Eq. (4), A_{LG} is the liquid–gas interfacial area and A_{SL} is the solid–liquid contact area. As illustrated in Fig. 1(a), A_{SG} denotes the total substrate area in the droplet-affected region, so that $A_{SG} - A_{SL}$ represents the part of this region that remains exposed to the gas phase. The remaining substrate area A_{SG}^{*} lies outside the droplet-affected region and is assumed to be independent of the droplet shape, wetting state, and applied electric field. Since both γ_{SG}^{*} and A_{SG}^{*} are independent of the variational variables considered here, the last term contributes only an additive constant to the total free energy and can be omitted in the following consideration.

For droplets with sufficiently small Bond numbers, gravitational deformation is negligible and the equilibrium shape can be approximated by a spherical cap.[38] Let r_c be the contact radius and θ be the apparent contact angle. The droplet volume then is

$$\Omega = \frac{\pi}{3}\left(\frac{r_c}{\sin\theta}\right)^3 (2+\cos\theta)(1-\cos\theta)^2. \tag{5}$$

For a prescribed droplet volume, this relation determines the contact radius as a function of the contact angle,

$$r_c = \left[\frac{3\Omega\sin^3\theta}{\pi(2+\cos\theta)(1-\cos\theta)^2}\right]^{1/3}. \tag{6}$$

The liquid–gas interfacial area and the solid–liquid contact area are given by

$$A_{LG} = 2\pi\left(\frac{r_c}{\sin\theta}\right)^2 (1-\cos\theta)$$

and

$$A_{SL} = \pi r_c^2.$$

Because the droplet volume is fixed, variations of A_{LG} and A_{SL} induced by a change in θ are not independent. Differentiating the above-mentioned geometrical relations at constant Ω gives

$$\left.\frac{\partial A_{LG}}{\partial\theta}\right|_{\Omega} = \cos\theta \left.\frac{\partial A_{SL}}{\partial\theta}\right|_{\Omega}. \tag{7}$$

After omitting constant terms, the shape-dependent part of the surface free energy becomes

$$E = \gamma_{LG}A_{LG} + (\gamma_{SL} - \gamma_{SG})A_{SL} + \text{const.} \tag{8}$$

The equilibrium contact angle is obtained from the following condition:

$$\frac{\mathrm{d}E}{\mathrm{d}\theta} = 0,$$

under the constraint of fixed droplet volume. Using Eq. (7), one obtains

$$\gamma_{LG}\cos\theta + \gamma_{SL} - \gamma_{SG} = 0$$

or, equivalently,

$$\cos\theta = \frac{\gamma_{SG} - \gamma_{SL}}{\gamma_{LG}}. \tag{9}$$

This is Young's equation, which expresses the equilibrium contact angle in terms of the balance among the liquid–gas, solid–liquid, and solid–gas interfacial free energies.

We next extend this classical argument to the standard electrowetting-on-dielectric configuration. Consider a conducting droplet placed on a metallic electrode coated by a dielectric layer of thickness d and dielectric permittivity ε_S, as schematically shown in Fig. 1. When an external voltage V is applied between the droplet and the electrode, the dielectric layer beneath the droplet behaves as a parallel-plate capacitor with capacitance,

$$C_S = \frac{\varepsilon_0\varepsilon_S}{d}A_{SL}. \tag{10}$$

The electrostatic energy stored in the dielectric layer is

$$U = \frac{1}{2}C_S V^2 = \frac{\varepsilon_0\varepsilon_S V^2}{2d}A_{SL}. \tag{11}$$

At fixed applied voltage, however, the appropriate thermodynamic potential must also include the work exchanged with the voltage source. The charge stored on the capacitor is

$$Q = C_S V = \frac{\varepsilon_0\varepsilon_S V}{d}A_{SL}, \tag{12}$$

and the work supplied by the voltage source is

$$W = QV = \frac{\varepsilon_0\varepsilon_S V^2}{d}A_{SL}. \tag{13}$$

Therefore, the voltage-controlled electrostatic contribution to the free energy is[8]

$$U - W = -\frac{1}{2}C_S V^2 = -\frac{\varepsilon_0\varepsilon_S V^2}{2d}A_{SL}.$$

This contribution can be absorbed into an effective voltage-dependent solid–liquid interfacial free-energy density,

$$\gamma_{SL}(V) = \gamma_{SL}(0) - \frac{\varepsilon_0\varepsilon_S V^2}{2d}. \tag{14}$$

Substituting Eq. (14) into Young's equation gives the classical Young–Lippmann equation,

$$\cos\theta(V) = \cos\theta_0 + \frac{\varepsilon_0\varepsilon_S V^2}{2d\gamma_{LG}}, \tag{15}$$

where θ_0 is the equilibrium contact angle at zero voltage. This term $c_S = \varepsilon_0\varepsilon_S/d$ in Eq. (15) represents the areal capacitance of the dielectric substrate, which is the same as c in Eq. (1). The Young–Lippmann equation predicts a quadratic increase in the cosine of the contact angle with the applied voltage, or equivalently a decrease in the apparent contact angle as the voltage increases.

This classical theory successfully describes the experimentally observed reduction in the droplet contact angle in the low-voltage

09 November 2026 06:57:17

© Author(s) 2026

regime.[17] However, experiments commonly show that the contact angle ceases to decrease once the voltage is increased beyond a certain range, a phenomenon known as contact-angle saturation. Further increasing the applied voltage may also induce additional instability and failure mechanisms, including droplet breakup, dielectric breakdown, and other irreversible electrohydrodynamic effects. These observations indicate that the classical Young–Lippmann description is incomplete at high voltage and motivate the generalized interfacial-energy framework developed in the following.

B. Surface composition effect on electrical energy

The adsorption-layer theory was first introduced by Wang and Nestler[39] and was subsequently applied to describe a range of wetting phenomena, including contact-angle hysteresis,[39] line tension,[38,40] and static friction of droplets.[33] A central implication of this framework is that the interfacial energy between two phases is not simply a prescribed constant, but rather a composition-dependent quantity determined by the local material composition within the adsorption layer. The idea was inspired by the surface excess description of Willard Gibbs[41] and the diffusion interface theory by Van der Waals.[42,43]

Both theories demonstrate the fact that an interface is not merely a geometrical boundary between two bulk phases, but a thermodynamic region with its own excess composition and excess free energy.[41] The interfacial tension is the reversible work required to create a unit interfacial area, and this work depends on the molecular composition and structure of the interfacial region.[42] If the molecules near the interface have a composition different from that of the bulk phases, their intermolecular interactions, entropy of mixing, local pressure, and density-gradient contribution are also different from those in the bulk. Consequently, changing the composition of this finite interfacial region changes the excess free energy per unit area, namely, the interfacial tension.

This connection is implicitly obtained in the Gibbs description of interfaces.[41] Although the Gibbs construction represents the interface by a mathematical dividing surface, the thermodynamic state of the interface is characterized by surface excess quantities. These surface excesses measure the amount of matter associated with the interfacial region relative to the extrapolated bulk phases, and their variation is directly coupled to the surface free energy through interfacial thermodynamics. Thus, even in the sharp-surface Gibbs formulation, the interface carries a composition-dependent thermodynamic state rather than being a purely geometrical discontinuity.

The same idea becomes more explicit in the van der Waals–Cahn diffuse-interface picture.[42–44] Van der Waals regarded the interface as a finite transition region in which density or composition varies continuously between two bulk phases. Cahn later formulated this view in terms of a free-energy functional containing both a homogeneous free-energy density and a gradient-energy penalty.

To account for the unresolved compositional transition between the solid-adjacent adsorption state and the corresponding bulk phase, we interpret the present adsorption-layer model in the framework of a Cahn-type diffuse-interface description. At the microscopic level, the free energy functional contains a local bulk contribution, a square-gradient penalty associated with spatial variations of composition, and a wall free-energy contribution,

$$\mathscr{F}[\varphi] = \int_\Omega \left[f_b(\varphi) + \frac{\kappa}{2}|\nabla\varphi|^2 \right] \mathrm{d}V + \int_{\partial\Omega_s} f_w(\varphi_s)\, \mathrm{d}A, \tag{16}$$

where φ is the local composition or concentration, $f_b(\varphi)$ is the homogeneous free-energy density, and κ is the gradient-energy coefficient. The same wall free-energy function $f_w(\varphi_s)$ is used in the liquid- and gas-covered regions, but is evaluated at the corresponding solid-adjacent states, ϕ_L and ϕ_G. In such a description, the interfacial tension is obtained by integrating the excess free-energy density across the finite inhomogeneous layer. Therefore, the value of the interfacial tension is determined not only by the two adjoining bulk phases but also by the composition profile and energetic state of the interfacial region itself. This provides the thermodynamic basis for representing the solid-adjacent region as an adsorption layer with a finite thickness and a composition variable.

To measure the energetic cost of continuously restoring the solid-adjacent state to the corresponding homogeneous bulk state, the integral of the excess free energy between the two states should also be included. Since this excess originates from the liquid-side and gas-side near-wall regions, respectively, it is naturally assigned to the effective solid–liquid and solid–gas interfacial free energies,[44]

$$\gamma_{Si}^{\mathrm{eff}} = f_w(\phi_i) + \int_{\phi_{\mathrm{bulk},i}}^{\phi_i} \sqrt{\kappa\alpha_i(\varphi - \phi_{\mathrm{bulk},i})^2}\,\mathrm{d}\varphi,$$
$$\alpha_i = \left.\frac{\partial^2 f_b}{\partial\varphi^2}\right|_{\varphi=\varphi_{bulk,i}}. \tag{17}$$

In the expression of surface energy density Eq. (17), the first part, f_w, which accounts for the on-site composition-dependent surface energy contribution could be formulated with the adsorption layer form. The contribution includes the interaction energy term, $\ell\chi(\phi)$, and the volumetric internal-energy density term, $\ell e(\phi)$, with ℓ representing the thickness of the adsorption layer. The detailed expressions of the terms are

$$\chi(\phi_i) = \chi_{LG}\phi_i(1-\phi_i) + \chi_{SL}\phi_i + \chi_{SG}(1-\phi_i),$$
$$e(\phi_i) = e_L\phi_i + e_G(1-\phi_i). \tag{18}$$

In this study, $i = L, G$, representing the liquid and gas phases, separately.

As for the non-local energetic contribution associated with the formation of the adsorption layer adjacent to the solid surface, a deviation of the solid-adjacent composition from its corresponding bulk value requires a spatial relaxation toward the homogeneous bulk state and, therefore, introduces an additional free-energy cost. A local Taylor expansion of the Cahn free-energy density about the bulk composition shows that, to leading order, this relaxation energy depends quadratically on the compositional mismatch. After coarse-graining the unresolved near-wall composition profile, the resulting contribution to the effective solid–fluid interfacial free energy can, therefore, be expressed as

$$\int_{\phi_{\mathrm{bulk},i}}^{\phi_i} \sqrt{\kappa\alpha_i(\varphi - \phi_{\mathrm{bulk},i})^2}\,\mathrm{d}\varphi \simeq \ell k_i(\phi_i - \phi_{\mathrm{bulk},i})^2, \tag{19}$$

where k_i is an effective coefficient describing the energetic cost of the unresolved compositional relaxation. In the ideal quadratic

09 November 2026 06:57:17

© Author(s) 2026

Cahn limit, k_i is related to κ and the quadratic coefficient α_i of the bulk free-energy expansion around the corresponding equilibrium composition and, therefore, depends on the local composition distribution. A detailed derivation is provided in Appendix. A.

Since the detailed composition or density profile near the solid surface and the three-phase contact line is generally difficult to determine, k_i is treated here as an effective parameter and its influence is examined parametrically. Its effective value may be affected by local surface geometry,[45] substrate deformation,[46] and the local electric-field and electric-stress distributions.[11,45,46]

The resulting solid–fluid interfacial free-energy density is, therefore, expressed as

$$\gamma_{Si}(\phi_i, V) = \ell\left[\chi(\phi_i) + e(\phi_i) + k_i(\phi_i - \phi_{\mathrm{bulk},i})^2\right] + g_{\mathrm{el},i}(\phi_i, V). \quad (20)$$

Here, the first two terms describe the local wall thermodynamics of the adsorption layer, while the additional quadratic term represents the free-energy cost associated with the unresolved relaxation from the solid-adjacent adsorption state to the adjoining homogeneous bulk phase. In addition, $g_{\mathrm{el}}(\phi, V)$ is the electrical related energy contribution determined later in Eq. (22). We define

$$f_i(\phi_i) = \chi(\phi_i) + e(\phi_i) + k(\phi_{\mathrm{bulk},i}, \phi_i) \quad (21)$$

as the volumetric chemical contribution to the free-energy density.

In electrowetting-on-dielectric (EWOD) systems, the material composition of the adsorption layer near the solid surface should not be neglected.[21,22,47,48] In the classical Young–Lippmann description, the electrical contribution is usually assigned to the liquid-covered part of the dielectric layer, which is treated as a capacitor with a fixed areal capacitance.[17] This assumption leads to the familiar quadratic reduction of the effective solid–liquid interfacial free energy with the applied voltage. However, such a description is incomplete once the finite interfacial structure near the solid surface is considered.[19] The electric field,[25] charge deposition,[49] ion injection,[13] and Maxwell stress[24] are not necessarily confined strictly within the macroscopic liquid footprint, and previous theoretical and numerical studies have shown that the electrically affected region near and outside the apparent three-phase contact line can also contribute to the electrowetting response.[50–52]

In addition to the dielectric coating, the solid-adjacent interfacial region may also contribute to the electrical free energy because its local composition, polarization, and charge-storage ability differ from those of the bulk phases. We, therefore, represent this unresolved interfacial electrical response through a composition-dependent effective capacitance associated with the adsorption layer. In this sense, the adsorption layer is not introduced as an additional macroscopic phase, but as a coarse-grained interfacial region whose electrical properties depend on the local wetting state.

We consider the total free energy of the system composed of the droplet, the dielectric coating, and the voltage source, where the voltage source is represented by a fixed-voltage boundary condition. The local state of the adsorption layer is described by an averaged liquid fraction ϕ. As a minimal approximation, the relative permittivity of the adsorption layer is taken as a linear interpolation between the gas-rich and liquid-rich limits,

$$\varepsilon_{\mathrm{a}}(\phi) = \varepsilon_G(1-\phi) + \varepsilon_L\phi.$$

For an adsorption layer of thickness ℓ, the corresponding areal capacitance is

$$c_{\mathrm{a}}(\phi) = \frac{\varepsilon_0\varepsilon_{\mathrm{a}}(\phi)}{\ell}.$$

Since the permittivity of the gas-rich state is much smaller than that of the liquid-rich state, this expression may be approximated as

$$c_{\mathrm{a}}(\phi) \simeq c_L\phi, \qquad c_L = \frac{\varepsilon_0\varepsilon_L}{\ell}.$$

The adsorption layer and the dielectric coating are then treated as two capacitive elements connected in series. The areal capacitance of the dielectric coating is

$$c_S = \frac{\varepsilon_0\varepsilon_S}{d},$$

where d is the dielectric thickness and ε_S is the relative permittivity of the dielectric material. The effective areal capacitance of the combined interfacial–dielectric structure is, therefore,

$$c_{\mathrm{eff}}(\phi) = \frac{c_S c_{\mathrm{a}}(\phi)}{c_S + c_{\mathrm{a}}(\phi)}.$$

Using $c_{\mathrm{a}}(\phi) \simeq c_L\phi$, this becomes

$$c_{\mathrm{eff}}(\phi) = \frac{c_S c_L\phi}{c_S + c_L\phi} = c_S\frac{\lambda\phi}{1+\lambda\phi},$$

where

$$\lambda = \frac{c_L}{c_S}.$$

In the main model, we first adopt the linear capacitive response. For a given local composition, ϕ, the effective surface charge density stored in the combined interfacial–dielectric capacitor is written as

$$\sigma(\phi, V) = c_{\mathrm{eff}}(\phi)V.$$

Because the voltage rather than the charge is externally prescribed, the relevant electrical contribution to the interfacial free energy is the constant-voltage free energy denoted by g_{el}. It is obtained from

$$g_{\mathrm{el}}(\phi, V) = -\int_0^V \sigma(\phi, V')\,\mathrm{d}V'. \quad (22)$$

For the linear response above, this gives

$$g_{\mathrm{el}}(\phi, V) = -\frac{1}{2}c_{\mathrm{eff}}(\phi)V^2.$$

In the present framework, the same expression can be applied to both the liquid-covered A_{SL} and the liquid-affected gas-covered $A_{SG} - A_{SL}$ regions, but with different local adsorption-layer compositions. For the two regions, we write

$$\sigma_i(\phi_i; V) = c_{\mathrm{eff},i}(\phi_i)V,$$
$$g_{\mathrm{el},i}(\phi_i; V) = -\frac{1}{2}c_{\mathrm{eff},i}(\phi_i)V^2,$$
$$i = L, G.$$

Here, ϕ_L and ϕ_G denote the averaged adsorption-layer compositions below the liquid-covered region and the liquid-affected gas-covered

09 November 2026 06:57:17

© Author(s) 2026

region, respectively. The electrical contribution to the apparent wetting behavior is, therefore, not determined only by the absolute electrical energy stored below the liquid footprint, but by the difference between the composition-dependent electrical free energies of the two interfacial regions.

It should be emphasized that the electrical response assigned to the gas-covered region is local. In the present model, $A_{SG} - A_{SL}$ represents only the droplet-affected transition region immediately outside the apparent three-phase contact line, whereas the far-field solid–gas region A_{SG}^{*} remains unaffected. The same externally imposed voltage V is, therefore, applied to the liquid-covered and locally affected gas-covered regions as a coarse-grained description of their electrical coupling. As the gas-side wetting state becomes liquid-rich, the electric-field contribution in this local region approaches that of the liquid-covered side, leading to the cancellation of their electrical free-energy difference at saturation. This local screening does not imply the formation of a macroscopically extended conductive film over the entire surrounding substrate.

The linear relation $\sigma(\phi, V) = c_{\mathrm{eff}}(\phi)V$ should be regarded as the lowest-order response of the adsorption layer. This approximation assumes that the ion distribution and polarization state in the liquid-rich interfacial region are not strongly modified by the applied voltage in a way that changes the effective dielectric response.

Under this assumption, the adsorption layer can be described by a composition-dependent but voltage-independent effective capacitance. In other words, the voltage dependence of the charge density enters mainly through the factor V, while the material dependence enters through $c_{\mathrm{eff}}(\phi)$.

More detailed interfacial charging models may lead to nonlinear charge–voltage relations,[18,20] including Gouy–Chapman-type descriptions for dilute electrolytes[21] and Kornyshev-type descriptions for concentrated electrolytes or ionic liquids.[22] Microscopic charging models are not considered in the present work. If required, they can readily be incorporated by replacing the linear relation $\sigma = c_{\mathrm{eff}}V$ with a more general response $\sigma(\phi, V)$, while the fixed-voltage electrical free-energy expression in Eq. (22) remains applicable.

This viewpoint is consistent with several existing interpretations of contact-angle saturation. In the charge-trapping model of Verheijen and Prins[8] and in ion-injection models,[13] ions transferred from the droplet into the surrounding medium modify the Maxwell stress and introduce an additional osmotic contribution at the interface, again indicating that the electrical driving force depends on the local composition and charge distribution of the interfacial region. These results suggest that the electrical contribution relevant to electrowetting should be regarded as an effective interfacial free-energy term controlled by the local composition and charge-storage state of the adsorption layer.

C. Construction of the adsorption-layer energy landscape

Having defined the composition-dependent interfacial free-energy densities, we now construct the adsorption-layer energy landscape used to determine the voltage-dependent wetting state. For a given applied voltage V, the liquid-covered and gas-covered parts of the droplet-affected substrate region are described by two averaged adsorption-layer compositions, ϕ_L and ϕ_G, respectively. Here, ϕ_L denotes the liquid fraction in the adsorption layer beneath the liquid footprint, while ϕ_G denotes the liquid fraction in the adsorption layer in the gas-covered but liquid-affected region. Since these two variables describe spatially distinct interfacial regions, they are not constrained by $\phi_L + \phi_G = 1$. The admissible composition space is, therefore,

$$0 \le \phi_L \le 1, \qquad 0 \le \phi_G \le 1.$$

For each pair (ϕ_L, ϕ_G), the corresponding solid–liquid and solid–gas interfacial free-energy densities are evaluated from the composition-dependent expressions introduced above,

$$\gamma_{SL} = \gamma_{SL}(\phi_L, V), \qquad \gamma_{SG} = \gamma_{SG}(\phi_G, V),$$

where both the chemical contribution and the constant-voltage electrical contribution are included. The apparent contact angle associated with this interfacial state is then determined by Young's relation, Eq. (9). Together with the fixed droplet volume, this contact angle determines the liquid–gas surface area and the solid–liquid contact area through the spherical-cap geometry given in Eqs. (5)–(8). Thus, the geometrical factors used in the total energy are not prescribed independently, but are obtained from the interfacial free-energy densities through the volume-conserving Young construction.

The total energy of the electrowetting system follows the expression of Eq. (4) and is then written as

$$E(\phi_L, \phi_G, V) = \gamma_{LG}A_{LG}(\theta) + A_{SL}(\theta)\gamma_{SL} + [A_{SG} - A_{SL}(\theta)]\gamma_{SG}. \quad (23)$$

This expression defines a two-dimensional energy landscape over the (ϕ_L, ϕ_G) plane for every applied voltage V.

The equilibrium adsorption-layer state is obtained by minimizing this energy landscape,

$$(\phi_L^{*}, \phi_G^{*}) = \underset{0\le\phi_L,\phi_G\le1}{\arg\min} \; E(\phi_L, \phi_G, V).$$

The minimum may occur either at an interior stationary point or on the boundary of the admissible composition space. Figure 2 illustrates the voltage-dependent evolution of the two-dimensional free-energy landscape $E(\phi_L, \phi_G, V)$. At low voltage, the global minimum is located close to the bulk-like configuration,

$$\phi_L = 1, \qquad \phi_G = 0,$$

corresponding to a liquid-rich adsorption layer beneath the droplet and a gas-rich adsorption layer outside the macroscopic liquid footprint.

An additional feature appears when the gas-side relaxation coefficient k_G is sufficiently small, as shown in Fig. 2(ii). In this case, the liquid-rich boundary $\phi_G = 1$ can become a second, metastable constrained minimum even when the global minimum remains at $\phi_G = 0$. The two states are then separated by an intermediate energy barrier. As the voltage is increased, the electrical contribution progressively stabilizes the liquid-rich gas-side adsorption state, and the global minimum eventually shifts from the low-ϕ_G state toward $\phi_G = 1$.

This distinction between global and local stability becomes important when a voltage cycle is considered. During voltage increase, the wetting state is assumed to evolve from the initially

09 November 2026 06:57:17

© Author(s) 2026

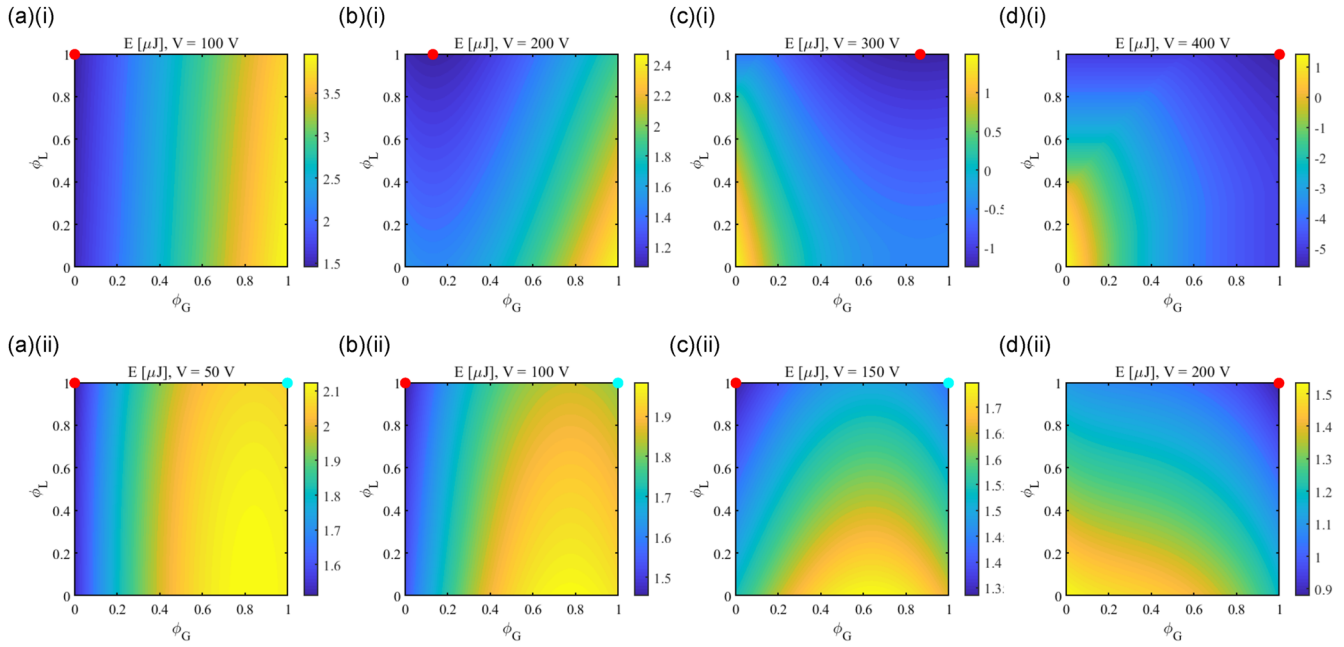


FIG. 2. Voltage-dependent evolution of the adsorption-layer free-energy landscape $E(\phi_L, \phi_G, V)$. Row (i) corresponds to ℓk_G = 0.04 J/m^2; row (ii) corresponds to ℓk_G = 0.01 J/m^2, with γ_{LG} = 72.3 mN/m corresponding to water. The red markers denote the global minimum, whereas the cyan markers indicate a secondary constrained local minimum when present. Row (i) illustrates the ordinary evolution toward the saturated state, while row (ii) illustrates the coexistence of low- and high-ϕ_G minima for sufficiently small k_G. (a) At low voltage, the global minimum is located close to the bulk-like state $(\phi_L, \phi_G) = (1, 0)$. For sufficiently small k_G, an additional constrained local minimum may also appear near the liquid-rich boundary $(\phi_L, \phi_G) = (1, 1)$, separated from the low-ϕ_G state by an energy barrier. [(b) and (c)] As the applied voltage increases, the relative stability of the gas-side adsorption states changes and the energetically preferred state shifts toward larger ϕ_G. (d) At sufficiently high voltage, the liquid-rich state $(\phi_L, \phi_G) = (1, 1)$ becomes energetically favored and represents the saturated adsorption-layer state. The coexistence of low- and high-ϕ_G local minima provides a possible thermodynamic origin of path dependence since the system may remain trapped in the high-ϕ_G basin during voltage reduction until the intervening energy barrier vanishes or is overcome.

09 November 2026 06:57:17

stable configuration by continuously following the global minimum of the free-energy landscape. During voltage reduction, however, a local minimum may coexist with the global minimum. The energy barrier separating these states can hinder the wetting state from returning to the global minimum-energy configuration, thereby delaying or preventing the receding transition. Such barrier-mediated trapping provides a possible mechanism for the hysteresis observed during voltage withdrawal.

A qualitatively similar macroscopic irreversibility has been reported for electrowetting on structured superhydrophobic surfaces.[46] In the thin-dielectric case shown in that work, the contact angle remained at the electrically induced value after the voltage was removed, whereas a much thicker dielectric allowed almost complete recovery.

III. RESULTS AND DISCUSSION

In this section, we discuss the main results and implications of the present energy-landscape framework for electrowetting-on-dielectric systems. We organize the analysis around four aspects: the modification of the classical Young–Lippmann response, the voltage-dependent evolution of the adsorption-layer energy landscape, the prediction of contact-angle saturation, and the comparison with experimental observations. Together, these results show that contact-angle saturation can emerge from the redistribution of the composition-dependent interfacial state, rather than from an imposed breakdown condition or a prescribed nonlinear charge law. The framework, therefore, provides a thermodynamic interpretation of electrowetting saturation in which the apparent contact angle is determined by the global minimum of the adsorption-layer energy landscape, while the applied voltage controls the transition between the Young–Lippmann-like regime, the interfacial transition regime, and the saturated regime.

A. Free-energy origin of Young–Lippmann behavior, transition, and saturation

The voltage-dependent electrowetting response obtained from the adsorption-layer energy landscape is summarized in Fig. 3.

Figure 3(a) shows the equilibrium contact angle as a function of the applied voltage. At low voltage, the minimum of the energy landscape is located at the bulk-like adsorption-layer state,

$$\phi_L^* = 1, \qquad \phi_G^* = 0.$$

In this regime, the gas-covered adsorption layer remains gas-rich and does not contribute appreciably to the electrical response. The

© Author(s) 2026

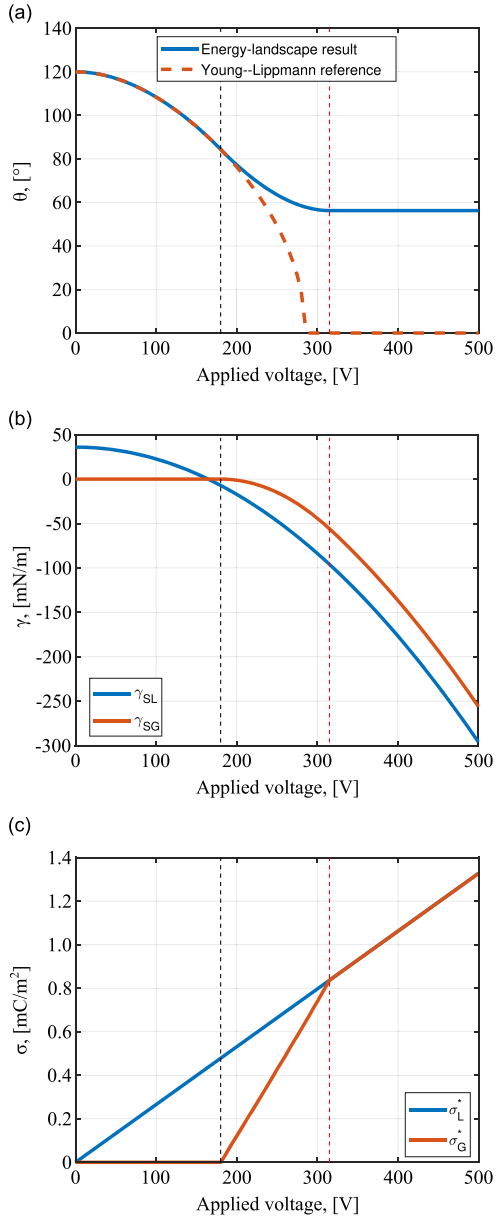


FIG. 3. Voltage-dependent electrowetting response obtained from the adsorption-layer energy landscape. (a) Equilibrium contact angle as a function of applied voltage. The solid curve is the energy-landscape result, and the dashed curve is the Young–Lippmann reference. At low voltage, the two curves coincide. The first vertical dashed line denotes the onset voltage V_{on}, where the energy minimum starts to leave the $\phi_G = 0$ boundary. The second vertical dashed line denotes the saturation voltage V_{sat}, where the minimum reaches $\phi_G = 1$. (b) Evolution of the effective interfacial free-energy densities, γ_{SL} and γ_{SG}, with the initial value of γ_{SG} taken as the reference. Before V_{on}, γ_{SL} decreases approximately according to the Young–Lippmann form, while γ_{SG} remains nearly unchanged. After V_{on}, γ_{SG} also decreases as the gas-covered adsorption layer becomes electrically active. After V_{sat}, γ_{SL} and γ_{SG} decrease synchronously, leaving an approximately constant interfacial-energy contrast. (c) Surface charge densities accumulated in the liquid-covered and gas-covered adsorption layers. The gas-side charge density starts to increase after V_{on} and follows the same liquid-rich capacitive response as the liquid-covered region after V_{sat}.

model, therefore, reduces to the classical Young–Lippmann behavior, and the contact angle follows the Young–Lippmann reference curve.

The first vertical dashed line shown in Fig. 3 marks the onset voltage V_{on}. As shown in Appendix B, this voltage is obtained from the boundary condition at $\phi_G = 0$,

$$\left.\frac{\partial \gamma_{SG}}{\partial \phi_G}\right|_{\phi_G=0} = 0.$$

For the linear capacitance model, this gives

$$V_{on}^2 = \frac{2\ell a_G}{c_S \lambda}. \tag{24}$$

Here, a_G collects the non-electrical linear contribution to the gas-side adsorption-layer free energy, c_S is the dielectric capacitance per unit area, and λ is the effective capacitance ratio of the gas-covered adsorption layer. When $V > V_{on}$, the energy minimum leaves the boundary $\phi_G = 0$, indicating that the gas-covered adsorption layer starts to become liquid-rich. This marks the beginning of the deviation from the Young–Lippmann prediction.

The second vertical dashed line marks the saturation voltage V_{sat}. This voltage corresponds to the point at which the energy minimum reaches the upper boundary,

$$\phi_G^* = 1.$$

As derived in Appendix B, V_{sat} is obtained from

$$\left.\frac{\partial \gamma_{SG}}{\partial \phi_G}\right|_{\phi_G=1} = 0,$$

which gives

$$V_{sat}^2 = \frac{2\ell(a_G + 2q_G)(1+\lambda)^2}{c_S \lambda}. \tag{25}$$

Here, $q_G = k_G - \chi_{LG}$ describes the quadratic stiffness of the gas-side adsorption-layer free energy. After this voltage, the gas-covered adsorption layer has reached the fully liquid-rich state allowed by the model. Further increases in V can no longer increase ϕ_G, and therefore, the contact angle enters the saturation regime.

The physical origin of this behavior is clarified by the interfacial free-energy densities shown in Fig. 3(b). In this plot, γ_{SG} is taken as the reference at zero voltage. Before V_{on}, the liquid-covered region follows the Young–Lippmann-like electrical response. Thus, γ_{SL} decreases approximately as a quadratic function of voltage,

$$\gamma_{SL}(V) \simeq \gamma_{SL}(0) - \frac{1}{2} c_{\mathrm{eff},L}(1) V^2,$$

whereas γ_{SG} remains nearly unchanged because the gas-covered adsorption layer is still close to $\phi_G = 0$. As a result, the contrast $\gamma_{SG} - \gamma_{SL}$ increases with voltage, and the apparent contact angle decreases.

Once V_{on} is exceeded, the gas-covered adsorption layer begins to participate in charge storage. Consequently, γ_{SG} also starts to decrease with voltage. The electrical reduction in γ_{SG} weakens the growth of the contrast $\gamma_{SG} - \gamma_{SL}$, and the contact-angle curve deviates from the Young–Lippmann reference. This regime corresponds

09 November 2026 06:57:17

© Author(s) 2026

to the transition region in which the energy minimum moves through the interior of the (ϕ_L, ϕ_G) energy landscape.

After V_{sat}, both adsorption-layer states are liquid-rich. The two interfacial free-energy densities then contain the same limiting electrical contribution,

$$\gamma_{SL}(V) = \ell f_L(1) - \frac{1}{2} c_{\mathrm{eff},L}(1) V^2,$$
$$\gamma_{SG}(V) = \ell f_G(1) - \frac{1}{2} c_{\mathrm{eff},G}(1) V^2.$$

When the limiting capacitances are identical,

$$c_{\mathrm{eff},G}(1) = c_{\mathrm{eff},L}(1),$$

the voltage-dependent electrical terms cancel in the Young relation. Thus,

$$\gamma_{SG}(V) - \gamma_{SL}(V) = \ell[f_G(1) - f_L(1)].$$

Using the present adsorption-layer free-energy form, one has

$$f_G(1) - f_L(1) = k_G.$$

Therefore, the saturated contact angle is

$$\cos\theta_{\mathrm{sat}} = \frac{\ell k_G}{\gamma_{LG}}. \tag{26}$$

This expression shows that the saturated contact angle is controlled by the terminal adsorption-layer energy penalty, while V_{sat} controls only the voltage at which this terminal state is reached. Contact-angle saturation, manifested as a deviation from the Young–Lippmann relation in Eq. (1), has been observed in numerous experiments.[1,7,8]

Figure 3(c) shows the corresponding accumulated surface charge densities. Before V_{on}, the charge density grows mainly in the liquid-covered region,

$$\sigma_L(V) \simeq c_{\mathrm{eff},L}(1) V,$$

while the gas-side charge density remains close to zero. After V_{on}, the increase in ϕ_G makes the gas-covered region electrically active and σ_G starts to grow. When V_{sat} is reached, both regions are in the liquid-rich limiting state, so that

$$\sigma_G(V) \simeq \sigma_L(V),$$

up to the same limiting capacitance response. The synchronous increase in σ_L and σ_G after saturation is consistent with the synchronous decrease in γ_{SL} and γ_{SG}, as shown in Fig. 3(b). Therefore, the saturation of the apparent contact angle is not caused by the disappearance of electrical energy. Instead, it results from the cancellation of the voltage-dependent electrical contributions in the interfacial-energy difference that determines the Young contact angle.

B. Parameter discussion and comparison with experiments

According to Eq. (26), decreasing k_G increases the saturated contact angle. The value of k_G also determines the topology of the free-energy landscape. At zero voltage, the gas-side interfacial free energy can be written, apart from an additive constant, as

$$\gamma_{SG}(\phi_G, 0) = \ell\left(a_G\phi_G + q_G\phi_G^2\right), \qquad q_G = k_G - \chi_{LG}. \tag{27}$$

Because $0 \le \phi_G \le 1$, both $\phi_G = 0$ and $\phi_G = 1$ are locally stable boundary states when

$$a_G > 0, \qquad a_G + 2q_G < 0. \tag{28}$$

The second condition gives

$$k_G < k_{G,c} = \chi_{LG} - \frac{a_G}{2}. \tag{29}$$

Below this critical value, the low- and high-ϕ_G minima are separated by an interior energy maximum. For the parameter set used here, the high-ϕ_G minimum persists to $V = 0$ when

$$\frac{\ell k_G}{\gamma_{LG}} \lesssim 0.09. \tag{30}$$

Therefore, reducing k_G not only increases the saturated contact angle but also stabilizes the liquid-rich state near $(\phi_L, \phi_G) = (1, 1)$.

These two effects illustrated in Fig. 4(a) compare the measurements of Chevalliot *et al.*[7] with theoretical curves calculated using the same k_G for different dielectric thicknesses. Changing the dielectric thickness modifies $c_S = \varepsilon_0\varepsilon_S/d$ and, therefore, shifts the voltage response, while the curve shape and saturated angle remain nearly unchanged. This explains why the thickness-dependent responses can be represented using the reduced voltage V/V_{sat} when the interfacial relaxation state is unchanged.

For soft dielectric substrates, however, changing the thickness also changes the electric-field distribution, electric stresses, and substrate deformation near the contact-line region, thereby modifying k_G. Figure 4(b) shows the measurements of Markodimitrakis *et al.*[45] for water on substrates with the same elastic modulus, $E = 40$ kPa. The saturation angle increases from ~54° at $d = 50$ μm to 60° at $d = 20$ μm and 82° at $d = 7$ μm. Within the present model, this thickness-dependent terminal state corresponds to a reduction in the effective k_G. A similar dependence on the interfacial material is observed by Chevalliot *et al.*, where Parylene-C and Parylene-HT coated with Fluoropel show similar terminal angles, whereas replacing Fluoropel by Cytop increases the saturation angle by ~10°. These results show that within the present coarse-grained representation, these changes can be represented by a variation of the effective k_G. Here, k_G is not introduced as an arbitrary voltage-dependent fitting parameter in the equilibrium calculations; for a given material/interfacial state, it is held fixed. Changes in k_G between systems are used only when the underlying interfacial or mechanical state is physically changed.

In the unresolved interfacial structure, local electric-field distribution, substrate-scale wetting configuration, and transitions between Cassie-like and Wenzel-like states[46] can alter the excess free-energy contribution and, therefore, be represented by a change in the effective coefficient k_G. Notice that the unloading process is not governed by k_G alone, but also by the combined interfacial parameters as in Eq. (29).

The two representative cases shown in Fig. 2 illustrate the corresponding limiting behaviors. For the parameter set in row (i),

09 November 2026 06:57:17

© Author(s) 2026

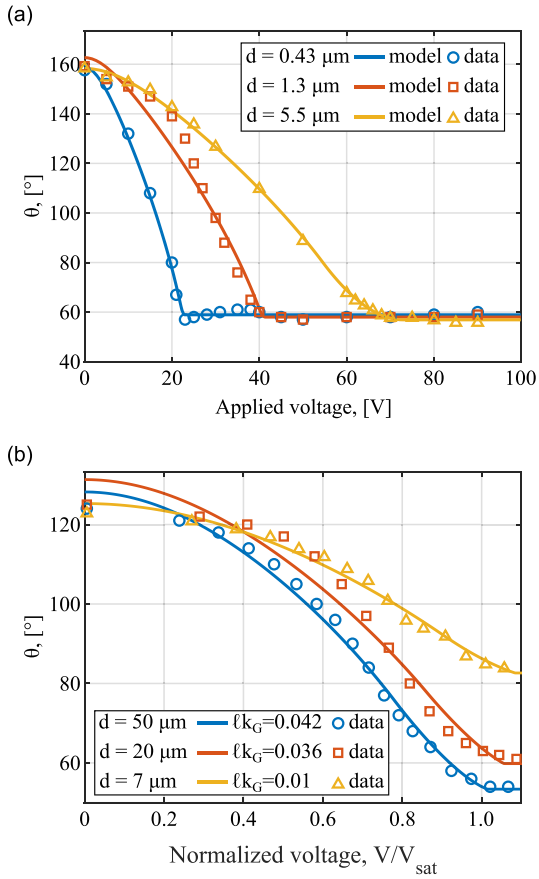


FIG. 4. Influence of dielectric thickness and the effective gas-side relaxation coefficient k_G on the electrowetting response. (a) Electrowetting curves for different dielectric thicknesses at fixed $\ell k_G = 0.005$ J/m^2, compared with experimental data from Chevalliot *et al.*[7] with $\gamma_{LG} = 10$ mN/m. Changing the dielectric thickness mainly shifts the voltage scale through the dielectric capacitance, while the curve shape and saturated contact angle remain similar. (b) Water electrowetting on soft dielectric films with $E = 40$ kPa and different thicknesses, using data from Markodimitrakis *et al.*[45] After normalization by V_{sat}, the different terminal angles are interpreted here as variations of the effective k_G caused by coupled electric-field and substrate-deformation effects.

the high-ϕ_G state does not remain metastable during voltage reduction, so that the system can return to the initial low-ϕ_G state. For the smaller-k_G case in row (ii), a second minimum persists near $(\phi_L, \phi_G) = (1, 1)$ and is separated from the low-ϕ_G state by an energy barrier, allowing the wetting state to remain trapped during voltage withdrawal. Such contrasting behavior is consistent with the experiments of Kavousanakis *et al.*[46] on structured superhydrophobic substrates. For example, a 75 μm SU8 dielectric exhibited recovery of the apparent contact angle from ~119° under actuation to 156° after the applied voltage was removed. However, for a 1 μm PMMA dielectric coated with a 0.4 μm TEOS layer, the contact angle changed from ~156°–111° at 65 V and remained close to 111° after the voltage was removed.

Therefore, k_G controls both the terminal contact angle and the stability of the liquid-rich adsorption-layer state: dielectric thickness mainly rescales the voltage response when k_G remains unchanged, whereas modifications of the local interfacial structure change k_G, leading to different saturation angles and, for sufficiently small k_G, a metastable state and electrowetting hysteresis.

Overall, the present framework provides an energy-landscape description of the electrowetting process. Within this description, the entire voltage-dependent contact-angle curve can be determined from a single set of interfacial parameters, as shown in Fig. 5. The initial equilibrium contact angle is fixed by the zero-voltage interfacial energy contrast, which is determined by the chemical and adsorption-layer parameters, such as χ_{LG}, χ_{SL}, χ_{SG}, e_L, and e_G. The initial decrease in the contact angle follows the Young–Lippmann-like response, with an effective capacitance determined by the dielectric layer and the adsorption-layer charge-storage ability. The deviation voltage V_{on}, the saturation voltage V_{sat}, and the saturated contact angle θ_{sat} are then obtained from the same energy minimization condition. Therefore, the initial state, the Young–Lippmann-like regime, the deviation from the classical prediction, the transition regime, and the final saturated state are all connected within one continuous theoretical curve.

This consistent description also clarifies the physical origin of contact-angle saturation. In the classical Young–Lippmann picture, the electrical contribution is assigned only to the liquid-covered region, so that the interfacial energy contrast continues to change quadratically with voltage. In the present model, the gas-covered but liquid-affected adsorption layer can also become electrically active. After the onset voltage, the gas-side adsorption state evolves toward a liquid-rich state and the electrical free energy of the gas-covered region begins to decrease together with that of the

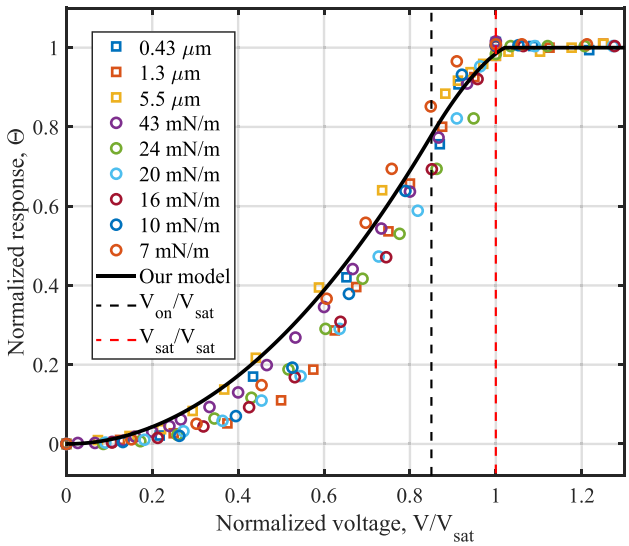


FIG. 5. Normalized comparison between the present model and the experimental data of Chevalliot *et al.*[7] The voltage is normalized by V_{sat} and the contact-angle response by the total change in cos θ. The comparison illustrates the consistency of the normalized experimental trends with the response predicted by using the present model.

09 November 2026 06:57:17

© Author(s) 2026

liquid-covered region. Once the gas-side adsorption layer reaches its limiting liquid-rich state, the two interfacial regions acquire the same limiting capacitive response. The difference between γ_{SG} and γ_{SL} then becomes voltage-independent, and the apparent contact angle reaches a saturated value.

A notable consequence of Eq. (26) is that the dielectric capacitance does not directly determine the saturated contact angle. For a fixed interfacial relaxation coefficient k_G, changing the dielectric thickness modifies c_S and, therefore, shifts V_{on} and V_{sat}, while the terminal contact angle remains unchanged. This limiting behavior is consistent with electrowetting systems in which the interfacial material state is insensitive to dielectric thickness.

The latter condition need not hold universally. When a change of dielectric thickness also modifies local electric stresses, substrate deformation, surface morphology, or the microscopic wetting state, the unresolved interfacial relaxation represented by the effective coefficient k_G may also change. In such systems, the dielectric thickness can, therefore, influence θ_{sat} indirectly through k_G, rather than through the capacitance term alone. The present model consequently distinguishes a purely capacitive thickness effect, which controls the voltage scale, from a coupled mechanical–interfacial thickness effect, which may additionally modify the terminal energy contrast.

Changing γ_{LG} affects the capillary normalization of the contact angle. However, the parameter k should also be related to the energetic cost of forming an adsorption-layer state opposite to the surrounding bulk phase. Since both processes are associated with creating a local liquid–gas-like interfacial mismatch inside the adsorption layer, their energetic cost is expected to scale with the liquid–gas interfacial energy. Consequently, if ℓk_G varies approximately in proportion to γ_{LG}, the ratio $\ell k_G/\gamma_{LG}$ remains nearly unchanged, leading to a weak variation of the saturated contact angle even when the liquid–gas surface tension is modified.

To compare different experiments on the same theoretical basis, we introduce the normalized variables,

$$\tilde{V} = \frac{V}{V_{\mathrm{sat}}}, \qquad \Theta = \frac{\cos\theta - \cos\theta_0}{\cos\theta_{\mathrm{sat}} - \cos\theta_0}.$$

Here, $\Theta = 0$ corresponds to the initial state and $\Theta = 1$ corresponds to the saturated state. Figure 5 compares the normalized theoretical curve with the experimental data reported by Chevalliot *et al.*,[7] where the contact-angle saturation was examined by varying either the dielectric thickness or the liquid–gas interfacial tension. Although the raw contact-angle curves have different voltage scales, the normalized data collapse onto the same theoretical transition curve. The normalized comparison shows that these experimental responses can be represented on a common voltage and contact-angle scale within the present formulation. Within the present model, this representation separates the parameters controlling the voltage scale from those controlling the terminal interfacial-energy contrast. In this sense, the energy-landscape framework provides a consistent description of the transition from the low-voltage Young–Lippmann-like regime to the saturated state. The normalized collapse should not be regarded as a discriminating validation of the present mechanism because different saturation models can display similar normalized responses. Its purpose here is only to demonstrate the consistency of the proposed energy-landscape pathway with the measured voltage scale and limiting states.

IV. CONCLUSION

In this work, we developed an energy-landscape framework for contact-angle saturation in electrowetting-on-dielectric systems. The central idea is that the electrical contribution to wetting should not be assigned only to the liquid-covered dielectric area. Instead, the liquid-covered region and the liquid-affected gas-covered region are treated on the same thermodynamic footing through composition-dependent adsorption-layer states. The local adsorption-layer composition determines both the non-electrical interfacial free energy and the effective capacitive response, so that the apparent contact angle is obtained from the global minimum of the total interfacial energy landscape.

Within this framework, the classical Young–Lippmann equation is recovered as the low-voltage limiting case. At low voltage, the energy minimum remains close to the bulk-like state, with a liquid-rich adsorption layer beneath the droplet and a gas-rich adsorption layer outside the liquid footprint. In this regime, the gas-covered region contributes negligibly to the electrical response and the contact angle decreases approximately according to the Young–Lippmann relation. As the voltage increases, the electrical contribution changes the stability of the gas-covered adsorption-layer state. The energy minimum then leaves the gas-rich boundary, leading to a deviation from the Young–Lippmann prediction.

The same model also predicts the saturation regime. When the gas-covered adsorption layer reaches its liquid-rich limiting state, the liquid-covered and gas-covered regions acquire the same limiting capacitive response. The voltage-dependent electrical terms then decrease synchronously in the two interfacial free energies and cancel in the interfacial-energy contrast that determines the Young contact angle. Thus, contact-angle saturation does not require the disappearance of electrical energy or an imposed nonlinear charge law. Rather, it results from the bounded evolution of the adsorption-layer state and the consequent saturation of the interfacial-energy contrast. For the quadratic adsorption-layer free energy used here, the saturated contact angle is given by

$$\cos\theta_{\mathrm{sat}} = \frac{\ell k_G}{\gamma_{LG}}.$$

This relation shows that the saturated angle is controlled by the terminal adsorption-layer energy contrast, whereas the dielectric capacitance mainly controls the voltage scale required to reach the deviation and saturation points. The present framework provides a single energy-minimization description of the low-voltage Young–Lippmann-like response, the onset of deviation, the transition regime, and the terminal saturated state. The corresponding onset voltage, saturation voltage, and saturated contact angle follow from the same set of interfacial state variables and model parameters. Comparison with experimental data for different dielectric thicknesses and liquid–gas interfacial tensions shows that the normalized responses are consistent with the transition behavior predicted by the model. This comparison is not intended to distinguish the present mechanism from other saturation mechanisms, but rather to assess whether the proposed energy-landscape description can reproduce the observed voltage and contact-angle scales.

The present model is intentionally formulated at the level of an effective interfacial free energy. Microscopic details such as nonlinear double-layer charging, ion-specific adsorption, charge trapping,

09 November 2026 06:57:17

© Author(s) 2026

leakage, or dielectric failure can be incorporated through more detailed constitutive relations for the effective charge response. However, these effects are not required for the basic saturation mechanism identified here. The results show that within the assumptions of the present model, contact-angle saturation can arise from the voltage-induced evolution of the adsorption-layer composition and the resulting saturation of the interfacial-energy contrast. This provides a thermodynamic pathway connecting the low-voltage Young–Lippmann-like regime to the high-voltage saturated state.

The present analysis treats the effective coefficients k_i as constants throughout a complete voltage loading–unloading cycle, corresponding to a fixed interfacial structure within an equilibrium or quasi-equilibrium description. In realistic systems, however, the effective k_i may evolve with the applied voltage and loading history, particularly for soft[45] or structured substrates,[46] where electromechanical deformation or transitions between Cassie- and Wenzel-like wetting states can substantially modify the local geometry and compositional relaxation represented by k_i. Describing such history-dependent evolution would require additional structural or kinetic state variables and, therefore, lies beyond the scope of the present equilibrium framework.

The present single-droplet description also does not account for high-voltage instabilities, such as droplet breakup[53] and dielectric breakdown.[11,52] Once breakup occurs, multiple metastable morphological states may coexist, with their free energies depending on the number of daughter droplets, their relative sizes, interfacial areas, and topology, thereby introducing substantially more degrees of freedom than those considered in the present model. Furthermore, the current framework is formulated for quasi-static voltage actuation and does not describe the frequency-dependent response associated with alternating-current electrowetting.[54,55] Extensions incorporating voltage- and history-dependent interfacial evolution, morphological transitions and breakup, and time-dependent electrical forcing constitute natural directions for future development of the present energy-landscape framework.

ACKNOWLEDGMENTS

R.Y. acknowledges the Gottfried-Wilhelm Leibniz prize under Grant No. NE 822/31-1 of the German Research Foundation (DFG) for providing funding of the research. F.W. acknowledges VirtMat project "VirtMat P09: Wetting Phenomena" of the Helmholtz association for providing funding as part of the program "MSE-materials science and engineering" under Grant No. 43.31.01.

AUTHOR DECLARATIONS

Conflict of Interest

The authors have no conflicts to disclose.

Author Contributions

Ruize Yin: Conceptualization (equal); Data curation (lead); Formal analysis (lead); Investigation (equal); Methodology (equal); Validation (equal); Visualization (equal); Writing – original draft (lead). **Fei Wang**: Conceptualization (lead); Investigation (equal); Methodology (equal); Supervision (equal); Validation (equal); Visualization (equal); Writing – original draft (supporting); Writing – review & editing (equal). **Britta Nestler**: Project administration (lead); Resources (lead); Writing – review & editing (equal).

DATA AVAILABILITY

No new experimental data were generated in this study. The experimental data used for comparison were taken from the cited literature. The data and MATLAB scripts that support the findings of this article are openly available in Github at https://github.com/Yin-Ruize/Electrowetting-Contact-Angle-Saturation-Induced-By-Surface-Composition.

NOMENCLATURE

A_{LG}	liquid–gas interfacial area (m^2)
A_{SG}	droplet-affected substrate area (m^2)
A_{SG}^*	far-field solid–gas area outside the droplet-affected region (m^2)
A_{SL}	liquid-covered solid–liquid contact area (m^2)
a_i	linear coefficient under the local stationarity condition for region $i = L, G$ ($J\ m^{-3}$)
$c_a(\phi)$	areal capacitance of the adsorption layer ($F\ m^{-2}$)
$c_{\mathrm{eff},i}(\phi)$	effective areal capacitance in region $i = L, G$ ($F\ m^{-2}$)
c_L	liquid-rich limiting adsorption-layer capacitance ($F\ m^{-2}$)
c_S	areal capacitance of the dielectric layer ($F\ m^{-2}$)
d	thickness of the dielectric layer (m)
E	total free energy of the droplet–substrate system (J)
$e(\phi_i)$	internal-energy contribution in the adsorption layer ($J\ m^{-3}$)
e_L, e_G	liquid-state and gas-state internal-energy coefficients ($J\ m^{-3}$)
$f_i(\phi_i)$	volumetric chemical contribution to the free-energy density in region $i = L, G$ ($J\ m^{-3}$)
$g_{\mathrm{el}}(\phi, V)$	constant-voltage electrical free-energy density ($J\ m^{-2}$)
$k(\phi_{\mathrm{bulk},i}, \phi_i)$	energy penalty for deviation from the adjacent bulk composition ($J\ m^{-3}$)
k_i	effective volumetric relaxation coefficient for region $i = L, G$ ($J\ m^{-3}$)
ℓ	thickness of the adsorption layer (m)
q_i	quadratic coefficient under the local stationarity condition for region $i = L, G$ ($J\ m^{-3}$)
r_c	contact radius of the droplet (m)
U	electrostatic energy stored in the capacitor (J)
V	applied voltage (V)
V_{on}	onset voltage at which the gas-side adsorption layer starts to leave the $\phi_G = 0$ boundary (V)
V_{sat}	saturation voltage at which the gas-side adsorption layer reaches $\phi_G = 1$ (V)
$\tilde{V}$	normalized voltage, $\tilde{V} = V/V_{\mathrm{sat}}$ (dimensionless)
W	work supplied by the voltage source (J)
θ	apparent contact angle (deg or°)
Θ	normalized electrowetting response, $\Theta = (\cos\theta - \cos\theta_0)/(\cos\theta_{\mathrm{sat}} - \cos\theta_0)$ (dimensionless)
λ	capacitance ratios c_L/c_S (dimensionless)

09 November 2026 06:57:17

© Author(s) 2026

ϕ	normalized composition/order parameter, with $\phi = 0$ and $\phi = 1$ denoting the gas-rich and liquid-rich limiting interfacial states. (dimensionless)
$\phi_G^*(V)$	energy-minimizing gas-side adsorption-layer interfacial state at voltage V (dimensionless)
$\phi_G^{\mathrm{int}}(V)$	interior gas-side stationary solution for $V_{\mathrm{on}} < V < V_{\mathrm{sat}}$ (dimensionless)
$\phi_L^*(V)$	energy-minimizing liquid-side adsorption-layer interfacial state at voltage V (dimensionless)
χ_{LG}	liquid–gas interaction coefficient in the adsorption layer (J m^{-3})
χ_{SG}	solid–gas interaction coefficient in the adsorption layer (J m^{-3})
χ_{SL}	solid–liquid interaction coefficient in the adsorption layer (J m^{-3})
$\chi(\phi_i)$	interaction contribution in the adsorption layer (J m^{-3})
Ω	droplet volume (m^3)
α_i	second derivative of the bulk free-energy density evaluated at phase $i = L, G$ (J m^{-3})
γ_{LG}	liquid–gas interfacial free-energy density (J m^{-2})
γ_{SG}	solid–gas interfacial free-energy density in the droplet-affected region (J m^{-2})
γ_{SG}^*	far-field solid–gas interfacial free-energy density (J m^{-2})
γ_{SL}	solid–liquid interfacial free-energy density (J m^{-2})
$\varepsilon_a(\phi)$	composition-dependent relative permittivity of the adsorption layer (dimensionless)
$\varepsilon_L, \varepsilon_G$	relative permittivities of the liquid-rich and gas-rich adsorption-layer limits (dimensionless)
ε_S	relative permittivity of the dielectric coating (dimensionless)
ε_0	vacuum permittivity (F m^{-1})
θ_{sat}	saturated contact angle (deg or°)
θ_0	equilibrium contact angle at zero voltage (deg or°)
$\theta^*(V)$	equilibrium contact angle obtained from the energy-minimizing adsorption-layer state at voltage V (deg or°)
σ	effective surface charge density (C m^{-2})
σ_L, σ_G	effective surface charge densities in the liquid-covered and gas-covered regions (C m^{-2})

APPENDIX A: CAHN-TYPE INTERPRETATION OF THE ADDITIONAL SOLID–FLUID INTERFACIAL CONTRIBUTION

The additional quadratic term introduced in the solid–fluid interfacial free energy can be interpreted from a Cahn-type diffuse-interface description. The purpose of the following derivation is not to resolve the full microscopic interfacial structure in the present macroscopic model, but to show how the unresolved compositional transition between the solid-adjacent adsorption state and the corresponding bulk phase produces an additional contribution to the effective solid–fluid interfacial free energy.

We consider a composition field $\varphi(\mathbf{r})$ described by the Cahn-type free-energy functional,[44,56]

$$\mathscr{F}[\varphi] = \int_\Omega \left[f_b(\varphi) + \frac{\kappa}{2}|\nabla\varphi|^2 \right] \mathrm{d}V + \int_{\Omega_s} f_w(\varphi_s)\, \mathrm{d}A, \tag{A1}$$

where $f_b(\varphi)$ is the homogeneous bulk free-energy density, κ is the square-gradient coefficient, and $f_w(\varphi_s)$ is the local wall free-energy density evaluated at the solid-adjacent composition φ_s.

Importantly, the same wall free-energy function $f_w(\varphi_s)$ is used on both sides of the contact line. The liquid-covered and gas-covered regions correspond to different values of the same surface state variable, such that

$$f_w(\varphi_s) = \begin{cases} f_w(\varphi_L), & \text{on the liquid-covered region,} \\ f_w(\varphi_G), & \text{on the gas-covered region.} \end{cases} \tag{A2}$$

Thus, the distinction between the solid–liquid and solid–gas regions does not require two different wall free-energy functions; it arises from the different solid-adjacent states φ_L and φ_G and from their connection to the corresponding liquid and gas bulk states.

For a wall-adjacent state relaxing toward the corresponding homogeneous bulk phase $i = L, G$, a local Taylor expansion around the equilibrium bulk composition gives, to leading order,

$$f_b(\varphi) \simeq f_b(\varphi_{b,i}) + \mu_{\mathrm{eq}}(\varphi - \varphi_{b,i}) + \frac{\alpha_i}{2}(\varphi - \varphi_{b,i})^2 + \mathscr{O}\left[(\varphi - \varphi_{b,i})^3\right], \tag{A3}$$

with

$$\mu_{\mathrm{eq}} = \left.\frac{\partial f_b}{\partial \varphi}\right|_{\varphi=\varphi_{b,i}}, \qquad \alpha_i = \left.\frac{\partial^2 f_b}{\partial \varphi^2}\right|_{\varphi=\varphi_{b,i}}. \tag{A4}$$

For an equilibrium one-dimensional relaxation profile normal to the interface, the Cahn equilibrium condition gives the local bulk excess and square-gradient contributions are equal at equilibrium, so that their sum is twice either contribution.[44] By converting the spatial coordinates to the composition coordinates, the additional interfacial free-energy cost associated with relaxation from the solid-adjacent state φ_i to the corresponding bulk state is, therefore,

$$\delta\gamma_i = \int_{\phi_{\mathrm{bulk},i}}^{\phi_i} \sqrt{\kappa\alpha_i(\varphi - \phi_{\mathrm{bulk},i})^2}\,\mathrm{d}\varphi. \tag{A5}$$

In the adsorption-layer model used in the main text, the microscopic solid-adjacent states are represented by the coarse-grained variables ϕ_L and ϕ_G. Accordingly, the additional relaxation contribution is written as

$$\delta\gamma_i \simeq \ell k_i(\phi_i - \phi_{\mathrm{bulk},i})^2, \qquad i = L, G. \tag{A6}$$

The local wall contribution employed in the present mean-field description is

$$f_w(\phi_i) = \ell[\chi(\phi_i) + e(\phi_i)], \qquad i = L, G, \tag{A7}$$

where the same functions $\chi(\phi)$ and $e(\phi)$ are evaluated at the different liquid- and gas-side adsorption states. Combining the local wall contribution with the unresolved diffuse relaxation gives

09 November 2026 06:57:17

© Author(s) 2026

$$\gamma_{Si}^{\mathrm{eff}} = \ell\left[\chi(\phi_i) + e(\phi_i) + k_i(\phi_i - \phi_{\mathrm{bulk},i})^2\right], \quad i = L, G. \tag{A8}$$

When the electrical contribution is included, we will obtain the interfacial free-energy density used in the main text.

The additional quadratic term, therefore, does not introduce a separate microscopic wall interaction. The local wall thermodynamics remains described by the same function $f_w(\phi)$, evaluated at ϕ_L or ϕ_G. The coefficient k_i instead represents the coarse-grained free-energy cost of the unresolved compositional relaxation between the solid-adjacent state and the corresponding homogeneous bulk state. The ordinary bulk liquid–gas transition is already contained in γ_{LG} and is, therefore, excluded from this additional solid–fluid contribution.

APPENDIX B: ANALYTICAL EXTREMA OF THE ADSORPTION-LAYER ENERGY LANDSCAPE

The extrema of the energy landscape can be obtained analytically from the local interfacial free-energy densities. For a given pair (ϕ_L, ϕ_G), the effective solid–liquid and solid–gas interfacial free-energy densities are written as

$$\gamma_{SL} = \gamma_{SL}(\phi_L, V), \qquad \gamma_{SG} = \gamma_{SG}(\phi_G, V).$$

The corresponding apparent contact angle is determined by the Young relation Eq. (9) Together with the fixed droplet volume, this relation determines the liquid–gas area $A_{LG}(\theta)$ and the solid–liquid area $A_{SL}(\theta)$, as given in Eqs. (5)–(8). The resulting total energy is given by Eq. (23).

In the normal spherical-cap regime, the geometry-induced terms in the derivatives with respect to ϕ_L and ϕ_G are canceled by the Young relation. Using

$$\frac{\mathrm{d}A_{LG}}{\mathrm{d}A_{SL}} = \cos\theta,$$

one obtains

$$\frac{\partial E}{\partial \phi_L} = A_{SL}\frac{\partial \gamma_{SL}}{\partial \phi_L},$$
$$\frac{\partial E}{\partial \phi_G} = (A_{SG} - A_{SL})\frac{\partial \gamma_{SG}}{\partial \phi_G}.$$

Thus, when $A_{SL} > 0$ and $A_{SG} - A_{SL} > 0$, the interior extrema of the full energy landscape satisfy

$$\frac{\partial \gamma_{SL}}{\partial \phi_L} = 0, \qquad \frac{\partial \gamma_{SG}}{\partial \phi_G} = 0.$$

The interfacial free-energy density of region $i = L, G$ is written as

$$\gamma_{Si}(\phi_i; V) = \ell f_i(\phi_i) - \frac{1}{2}c_{\mathrm{eff},i}(\phi_i)V^2,$$

where k_i is a volumetric energy density and is, therefore, multiplied by the adsorption-layer thickness ℓ. The linear effective capacitance is

$$c_{\mathrm{eff},i}(\phi_i) = c_S\frac{\lambda\phi_i}{1 + \lambda\phi_i},$$

and hence,

$$\frac{\mathrm{d}c_{\mathrm{eff},i}}{\mathrm{d}\phi_i} = c_S\frac{\lambda}{(1 + \lambda\phi_i)^2}.$$

For compactness, we define

$$a_i = \chi_{LG} + \chi_{SL} - \chi_{SG} + e_L - e_G - 2k_i\phi_{\mathrm{bulk},i},$$
$$q_i = k_i - \chi_{LG}.$$

Then,

$$\frac{\partial \gamma_{Si}}{\partial \phi_i} = \ell(a_i + 2q_i\phi_i) - \frac{1}{2}V^2\frac{\mathrm{d}c_{\mathrm{eff},i}}{\mathrm{d}\phi_i}.$$

The interior stationary condition is, therefore,

$$\ell(a_i + 2q_i\phi_i) = \frac{c_S\lambda V^2}{2(1 + \lambda\phi_i)^2}.$$

Equivalently, ϕ_i is determined by the following cubic equation:

$$0 = 2\ell q_i\lambda^2\phi_i^3 + \ell\left(a_i\lambda^2 + 4q_i\lambda\right)\phi_i^2 + \ell(2a_i\lambda + 2q_i)\phi_i + \ell a_i - \frac{1}{2}c_S\lambda V^2.$$

For the gas-covered region, $\phi_{\mathrm{bulk},G} = 0$, so that

$$a_G = \chi_{LG} + \chi_{SL} - \chi_{SG} + e_L - e_G,$$
$$q_G = k_G - \chi_{LG}.$$

The voltage-dependent gas-side adsorption state is then

$$\phi_G^*(V) = \begin{cases} 0, & V \le V_{\mathrm{on}}, \\ \phi_G^{\mathrm{int}}(V), & V_{\mathrm{on}} < V < V_{\mathrm{sat}}, \\ 1, & V \ge V_{\mathrm{sat}}, \end{cases}$$

where $\phi_G^{\mathrm{int}}(V)$ is the real root in $0 < \phi_G < 1$ of

$$0 = 2\ell q_G\lambda^2\phi_G^3 + \ell\left(a_G\lambda^2 + 4q_G\lambda\right)\phi_G^2 + \ell(2a_G\lambda + 2q_G)\phi_G + \ell a_G - \frac{1}{2}c_S\lambda V^2.$$

The onset voltage is obtained from the following boundary condition:

$$\left.\frac{\partial \gamma_{SG}}{\partial \phi_G}\right|_{\phi_G=0} = 0.$$

This gives Eq. (24), the voltage that the (θ, V) curve deviates from the Young–Lippmann relation.

Similarly, the local saturation voltage is obtained from

$$\left.\frac{\partial \gamma_{SG}}{\partial \phi_G}\right|_{\phi_G=1} = 0,$$

which gives the saturation voltage in Eq. (25).

Since

$$a_G + 2q_G = 2k_G - \chi_{LG} + \chi_{SL} - \chi_{SG} + e_L - e_G,$$

the saturation voltage can also be written as

09 November 2026 06:57:17

© Author(s) 2026

$$V_{\mathrm{sat}}^2 = \frac{2\ell[2k_G - \chi_{LG} + \chi_{SL} - \chi_{SG} + e_L - e_G](1+\lambda)^2}{c_S\lambda}.$$

The above-mentioned expressions give the local transition thresholds. For the global minimum, the admissible candidates,

$$\phi_G = 0, \qquad \phi_G = 1, \qquad \phi_G = \phi_{G,i}^{\mathrm{int}}(V),$$

are compared by their energy values. Here, $\phi_{G,i}^{\mathrm{int}}(V)$ denotes any real root of the cubic equation lying in $0 < \phi_G < 1$. The physically realized state is the candidate with the lowest total energy. This comparison also allows for discontinuous jumps when the global minimum switches between competing branches.

After the gas-covered adsorption layer reaches the liquid-rich boundary, one has

$$\phi_G^* = 1.$$

If the adsorption layer beneath the droplet remains liquid-rich, $\phi_L^* \simeq 1$ (as we have shown in the energy map), the saturated contact angle is obtained from

$$\cos\theta_{\mathrm{sat}} = \frac{\gamma_{SG}(1,V) - \gamma_{SL}(1,V)}{\gamma_{LG}}.$$

At $\phi = 1$, the non-electrical free-energy densities are

$$f_L(1) = \chi_{SL} + e_L,$$
$$f_G(1) = \chi_{SL} + e_L + k_G.$$

Therefore,

$$f_G(1) - f_L(1) = k_G.$$

The saturated-state Young relation becomes

$$\cos\theta_{\mathrm{sat}}(V) = \frac{\ell k_G}{\gamma_{LG}} - \frac{[c_{\mathrm{eff},G}(1) - c_{\mathrm{eff},L}(1)]V^2}{2\gamma_{LG}}.$$

In the fully liquid-rich limiting state, the two regions have the same limiting capacitance,

$$c_{\mathrm{eff},G}(1) = c_{\mathrm{eff},L}(1).$$

The voltage-dependent electrical contrast then cancels, giving Eq. (26),

$$\cos\theta_{\mathrm{sat}} = \frac{\ell k_G}{\gamma_{LG}}.$$

Thus, in this limiting regime, the saturated contact angle is determined by the terminal adsorption-layer energy contrast, while the applied voltage controls the voltage at which this terminal state is reached.

REFERENCES

[1] F. Mugele and J.-C. Baret, "Electrowetting: From basics to applications," J. Phys.: Condens. Matter **17**(28), R705 (2005).

[2] F. Mugele and J. Heikenfeld, *Electrowetting: Fundamental Principles and Practical Applications* (Wiley, 2018).

[3] K. H. Kang, "How electrostatic fields change contact angle in electrowetting," Langmuir **18**(26), 10318–10322 (2002).

[4] J. Buehrle, S. Herminghaus, and F. Mugele, "Interface profiles near three-phase contact lines in electric fields," Phys. Rev. Lett. **91**(8), 086101 (2003).

[5] F. Mugele and J. Buehrle, "Equilibrium drop surface profiles in electric fields," J. Phys.: Condens. Matter **19**(37), 375112 (2007).

[6] F. Mugele, "Fundamental challenges in electrowetting: From equilibrium shapes to contact angle saturation and drop dynamics," Soft Matter **5**(18), 3377–3384 (2009).

[7] S. Chevalliot, S. Kuiper, and J. Heikenfeld, "Experimental validation of the invariance of electrowetting contact angle saturation," J. Adhes. Sci. Technol. **26**(12–17), 1909–1930 (2012).

[8] H. J. J. Verheijen and M. W. J. Prins, "Reversible electrowetting and trapping of charge: Model and experiments," Langmuir **15**(20), 6616–6620 (1999).

[9] A. G. Papathanasiou and A. G. Boudouvis, "Manifestation of the connection between dielectric breakdown strength and contact angle saturation in electrowetting," Appl. Phys. Lett. **86**(16), 164102 (2005).

[10] A. G. Papathanasiou, A. T. Papaioannou, and A. G. Boudouvis, "Illuminating the connection between contact angle saturation and dielectric breakdown in electrowetting through leakage current measurements," J. Appl. Phys. **103**(3), 034901 (2008).

[11] A. I. Drygiannakis, A. G. Papathanasiou, and A. G. Boudouvis, "On the connection between dielectric breakdown strength, trapping of charge, and contact angle saturation in electrowetting," Langmuir **25**(1), 147–152 (2009).

[12] M. Vallet, M. Vallade, and B. Berge, "Limiting phenomena for the spreading of water on polymer films by electrowetting," Eur. Phys. J. B **11**(4), 583–591 (1999).

[13] T. Yamamoto, M. Doi, and D. Andelman, "Contact angle saturation in electrowetting: Injection of ions into the surrounding media," Europhys. Lett. **112**(5), 56001 (2015).

[14] V. Peykov, A. Quinn, and J. Ralston, "Electrowetting: A model for contact-angle saturation," Colloid Polym. Sci. **278**(8), 789–793 (2000).

[15] A. Quinn, R. Sedev, and J. Ralston, "Contact angle saturation in electrowetting," J. Phys. Chem. B **109**(13), 6268–6275 (2005).

[16] D. Klarman, D. Andelman, and M. Urbakh, "A model of electrowetting, reversed electrowetting, and contact angle saturation," Langmuir **27**(10), 6031–6041 (2011).

[17] E. Bormashenko and O. Gendelman, "A generalized electrowetting equation: Its derivation and consequences," Chem. Phys. Lett. **599**, 139–141 (2014).

[18] A. Quinn, R. Sedev, and J. Ralston, "Influence of the electrical double layer in electrowetting," J. Phys. Chem. B **107**(5), 1163–1169 (2003).

[19] M. Z. Bazant, K. Thornton, and A. Ajdari, "Diffuse-charge dynamics in electrochemical systems," Phys. Rev. E **70**(2), 021506 (2004).

[20] C. W. Monroe, L. I. Daikhin, M. Urbakh, and A. A. Kornyshev, "Electrowetting with electrolytes," Phys. Rev. Lett. **97**(13), 136102 (2006).

[21] D. L. Chapman, "LI. A contribution to the theory of electrocapillarity," London, Edinburgh, Dublin Philos. Mag. J. Sci. **25**(148), 475–481 (1913).

[22] A. A. Kornyshev, "Double-layer in ionic liquids: Paradigm change?," J. Phys. Chem. B **111**(20), 5545–5557 (2007).

[23] J. Park, X.-Q. Feng, and W. Lu, "Instability of electrowetting on a dielectric substrate," J. Appl. Phys. **109**(3), 034309 (2011).

[24] G. Linga, A. Bolet, and J. Mathiesen, "Controlling wetting with electrolytic solutions: Phase-field simulations of a droplet-conductor system," Phys. Rev. E **98**(1), 013101 (2018).

[25] H. Zhang, F. Wang, and B. Nestler, "Multi-component electro-hydro-thermodynamic model with phase-field method. I. Dielectric," J. Comput. Phys. **505**, 112907 (2024).

[26] J. Liu, M. Wang, S. Chen, and M. O. Robbins, "Uncovering molecular mechanisms of electrowetting and saturation with simulations," Phys. Rev. Lett. **108**(21), 216101 (2012).

[27] G. McHale, N. Gao, G. G. Wells, H. Barrio-Zhang, and R. Ledesma-Aguilar, "Friction coefficients for droplets on solids: The liquid–solid amontons' laws," Langmuir **38**(14), 4425–4433 (2022).

[28] G. Whyman, E. Bormashenko, and T. Stein, "The rigorous derivation of Young, Cassie–Baxter and Wenzel equations and the analysis of the contact angle hysteresis phenomenon," Chem. Phys. Lett. **450**(4), 355–359 (2008).

09 November 2026 06:57:17

© Author(s) 2026

[29]F. Wang, Y. Wu, and B. Nestler, "Wetting effect on patterned substrates," Adv. Mater. **35**(25), e2210745 (2023).
[30]P. G. De Gennes, "Wetting: Statics and dynamics," Rev. Mod. Phys. **57**(3), 827–863 (1985).
[31]H.-J. Butt, R. Berger, W. Steffen, D. Vollmer, and S. A. L. Weber, "Adaptive wetting—Adaptation in wetting," Langmuir **34**(38), 11292–11304 (2018).
[32]H. Zhang, H. Zhang, F. Wang, and B. Nestler, "Wetting effect induced depletion and adsorption layers: Diffuse interface perspective," Chem. Phys. Chem. **25**(14), e202400086 (2024).
[33]R. Yin, F. Wang, and B. Nestler, "A microscopic theory of small-droplet adhesion on solid surfaces," J. Chem. Phys. **165**(2), 024707 (2026).
[34]H. Teshima, T. Fukunaga, Q.-Y. Li, and K. Takahashi, "Precursor-film-driven ultra-early depinning of the three-phase contact line," J. Colloid Interface Sci. **678**, 1230–1238 (2025).
[35]Q. Yuan and Y.-P. Zhao, "Precursor film in dynamic wetting, electrowetting, and electro-elasto-capillarity," Phys. Rev. Lett. **104**(24), 246101 (2010).
[36]S. K. Bhaumik, M. Chakraborty, S. Ghosh, S. Chakraborty, and S. DasGupta, "Electric field enhanced spreading of partially wetting thin liquid films," Langmuir **27**(21), 12951–12959 (2011).
[37]R. Hennig, V. Cacucciolo, and H. Shea, "Actuating droplets with electrowetting: Force and dynamics," Droplet **3**(2), e108 (2024).
[38]F. Wang, H. Zhang, and B. Nestler, "Wetting phenomena: Line tension and gravitational effect," Phys. Rev. Lett. **133**(24), 246201 (2024).
[39]F. Wang and B. Nestler, "Wetting and contact-angle hysteresis: Density asymmetry and van der Waals force," Phys. Rev. Lett. **132**(12), 126202 (2024).
[40]F. Aurbach, F. Wang, and B. Nestler, "Microscopic origin of droplet line tension," J. Chem. Phys. **164**(24), 244702 (2026).
[41]J. Willard Gibbs, *The Collected Works of J. Willard Gibbs. Volume 1: Thermodynamics* (Longmans, Green and Co., New York, 1928), Vol. 1.
[42]J. D. Van der Waals and J. S. Rowlinson, *On the Continuity of the Gaseous and Liquid States* (Courier Corporation, 2004).
[43]J. D. Van Der Waals, "The thermodynamic theory of capillarity under the hypothesis of a continuous variation of density," J. Stat. Phys. **20**(2), 200–244 (1979).
[44]J. W. Cahn, "Critical point wetting," J. Chem. Phys. **66**(8), 3667–3672 (1977).
[45]I. E. Markodimitrakis, D. G. Sema, N. T. Chamakos, P. Papadopoulos, and A. G. Papathanasiou, "Impact of substrate elasticity on contact angle saturation in electrowetting," Soft Matter **17**(16), 4335–4341 (2021).
[46]M. E. Kavousanakis, N. T. Chamakos, K. Ellinas, A. Tserepi, E. Gogolides, and A. G. Papathanasiou, "How to achieve reversible electrowetting on superhydrophobic surfaces," Langmuir **34**(14), 4173–4179 (2018).
[47]L. Wang, X. Li, C. Li, Y. Qiu, Z. Wang, Q. Yang, H. Tian, C. Wang, X. Chen, and J. Shao, "Plasma-enhanced electrowetting-on-dielectrics," Appl. Phys. Lett. **125**(15), 151602 (2024).
[48]A. A. Papaderakis and R. A. W. Dryfe, "The renaissance of electrowetting," Curr. Opin. Electrochem. **38**, 101245 (2023).
[49]X. Li, A. D. Ratschow, S. Hardt, and H.-J. Butt, "Surface charge deposition by moving drops reduces contact angles," Phys. Rev. Lett. **131**, 228201 (2023).
[50]D. 't Mannetje, A. Banpurkar, H. Koppelman, M. H. G. Duits, D. van den Ende, and F. Mugele, "Electrically tunable wetting defects characterized by a simple capillary force sensor," Langmuir **29**(31), 9944–9949 (2013).
[51]G. Manukyan, J. M. Oh, D. van den Ende, R. G. H. Lammertink, and F. Mugele, "Electrical switching of wetting states on superhydrophobic surfaces: A route towards reversible Cassie-to-Wenzel transitions," Phys. Rev. Lett. **106**(1), 014501 (2011).
[52]Y. Xu, N. Morris, and Y. Wu, "Electrified EHL line contact with dielectric breakdown of lubricant—A numerical model," Tribol. Int. **217**, 110901 (2026).
[53]F. Mugele and S. Herminghaus, "Electrostatic stabilization of fluid microstructures," Appl. Phys. Lett. **81**(12), 2303–2305 (2002).
[54]F. Mugele, A. Klingner, J. Buehrle, D. Steinhauser, and S. Herminghaus, "Electrowetting: A convenient way to switchable wettability patterns," J. Phys.: Condens. Matter **17**(9), S559 (2005).
[55]Q. Lu, L. Wang, F. Li, Y. Yang, Q. Liu, X. Wang, F. Chi, L. Liu, and Z. Yi, "An electrohydrodynamic phase-field model for contact angle hysteresis in electrowetting pixels: Decoupling physical pinning and charge trapping," Micromachines **17**(4), 480 (2026).
[56]J. W. Cahn and J. E. Hilliard, "Free energy of a nonuniform system. I. Interfacial free energy," J. Chem. Phys. **28**(2), 258–267 (1958).

09 November 2026 06:57:17

© Author(s) 2026